

Hybrid Resource Allocation Scheme for Bistatic ISAC with Data Channels

Marcus Henninger, Lucas Giroto, Ahmed Elkelesh, Silvio Mandelli

Nokia Bell Labs Stuttgart, Germany

E-mail: {firstname.lastname}@nokia-bell-labs.com

Abstract—Bistatic integrated sensing and communication (ISAC) enables efficient reuse of the existing cellular infrastructure and is likely to play an important role in future sensing networks. In this context, ISAC using the data channel is a promising approach to improve the bistatic sensing performance compared to relying solely on pilots. One of the challenges associated with this approach is resource allocation: the communication link aims to transmit higher modulation order (MO) symbols to maximize the throughput, whereas a lower MO is preferable for sensing to achieve a higher signal-to-noise ratio in the radar image. To address this conflict, this paper introduces a hybrid resource allocation scheme. By placing lower MO symbols as pseudo-pilots on a suitable sensing grid, we enhance the bistatic sensing performance while only slightly reducing the spectral efficiency of the communication link. Simulation results validate our approach against different baselines and provide practical insights into how decoding errors affect the sensing performance.

Index Terms—ISAC, bistatic ISAC, bistatic sensing, payload sensing, OFDM, resource allocation, channel coding.

I. INTRODUCTION

As one of the key new features of the upcoming sixth generation (6G) standard, integrated sensing and communication (ISAC) is set to equip cellular networks with radar-like functionalities [1]. While the most important use cases such as drone and intrusion detection have largely been agreed on [2], [3] and research in both academia and industry has progressed rapidly in the last years, numerous challenges still remain to be addressed. Some of those are unique to bistatic ISAC systems [4], which offer great potential to reuse existing deployments and complement conventional monostatic setups.

In monostatic ISAC, an estimate of the sensing channel state information (CSI) matrix can be readily obtained via zero-forcing (ZF) element-wise division of the received frame by the transmitted frame in the discrete-frequency domain. In bistatic ISAC, either only pilots or the full frame can be used to estimate the sensing CSI matrix [5]. In the former case, the typically sparse pilot allocation leads to a limited sensing performance due to the associated reduction of the available processing gain and maximum unambiguous range and Doppler shift capabilities. Increasing the allocation density to counteract this leads to an undesired reduction in spectral efficiency for the communication link. While using the full frame allows circumventing this, its implementation in practice

This work has been submitted to the IEEE for possible publication. Copyright may be transferred without notice, after which this version may no longer be accessible.

is challenging since knowledge of the transmit symbols is typically not available at the receiver (RX), requiring to decode the data channel. However, also this results in a resource allocation conflict: sensing benefits from a low modulation and coding scheme (MCS) index (i.e., low modulation order (MO) and coding rate). This is due to the fact that lower MO symbols are less prone to transmission errors than higher MO symbols. As a consequence, they are still decodable at lower signal-to-noise ratio (SNR), which improves the bistatic sensing performance. Additionally, constant amplitude constellation symbols have the further benefit that they do not lead to noise enhancement when computing the CSI matrix via ZF [6] and exhibit lower sidelobes [7]. The communication link, on the other hand, aims at optimizing the spectral efficiency and would thus prioritize selecting the highest possible MCS to meet the target block error ratio (BLER).

The problem of sensing with the data channel in bistatic setups has been investigated in several studies. In [8], refined estimates of the target parameters and data are obtained after performing a coarse estimation of the target parameters using a Bayesian learning approach. The authors of [9] propose an iterative sensing and data demodulation approach, showing that the gap between pilot-only processing and a genie-aided scheme (i.e., perfect knowledge of the data symbols at the RX) can be narrowed. However, both works did not investigate the effects of channel coding present in practical systems. This aspect has been addressed in [5], where, among other aspects, the impact of decoding errors on the sensing performance has been studied. However, as in [8] and [9], the previously introduced resource allocation problem between sensing and communication was only addressed to the extent that different pilot densities and MOs were investigated. The use of superimposed pilots in [10] partially considers the aforementioned trade-off, but results in a power allocation problem involving a balance between pilots and information symbols. Furthermore, channel coding aspects were also not considered.

To close these gaps, we introduce a hybrid resource allocation scheme including channel coding for the data transmission, which addresses the previously introduced resource allocation conflict between communication and sensing. Specifically, we propose to allocate lower MO pseudo-pilots on a suitable grid for sensing predefined by sensing key performance indicators (KPIs). Our main contributions are as follows:

- We propose a hybrid resource allocation scheme that facilitates bistatic sensing while keeping the impact on

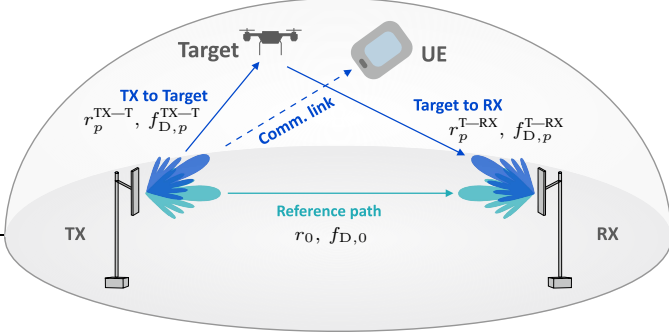


Fig. 1: Bistatic ISAC system model. In this example, a static reference path labeled as $p = 0$ and a path $p = 1$ associated with a radar target that is opportunistically illuminated by a transmission originally intended to an UE are shown. Here, $r_p = r_p^{TX-T} + r_p^{T-RX}$ is the bistatic range resulting from the sum of the range r_p^{TX-T} between TX and target and the range r_p^{T-RX} between target and RX. In addition, a Doppler shift $f_{D,p} = f_{D,p}^{TX-T} + f_{D,p}^{T-RX}$ is experienced.

the communication link minimal.

- Based on the proposed scheme, we detail the full processing pipeline to perform sensing at the bistatic RX, including channel coding aspects.
- We show by means of simulations that our hybrid resource allocation scheme enhances the bistatic sensing performance. Moreover, our results reveal practical insights about the impact of decoding errors on the sensing performance.

II. SYSTEM MODEL

We consider the bistatic ISAC system depicted in Fig. 1. The transmitter (TX) sends orthogonal frequency-division multiplexing (OFDM) symbols to a user equipment (UE) in the downlink (DL) for communication purposes, while the RX, e.g., a receive-only node, processes reflected signals to gain knowledge about objects in the environment.

The discrete-frequency domain TX frame, which consists of M OFDM symbols with N subcarriers that are spaced by Δf and carry complex modulation symbols, is denoted by $\mathbf{X} \in \mathbb{C}^{N \times M}$ and transmitted at carrier frequency f_c . The received frame $\mathbf{Y} \in \mathbb{C}^{N \times M}$ at the bistatic RX is

$$\mathbf{Y} = \mathbf{XH} + \mathbf{Z}, \quad (1)$$

where $\mathbf{Z} \in \mathbb{C}^{N \times M}$ is the random complex additive white Gaussian noise (AWGN) matrix, whose elements follow a Gaussian distribution with zero-mean and variance $\sigma_n^2 = P_n/N$, with P_n being the noise power over the whole bandwidth. We model the channel frequency response (CFR) as a superposition of a strong path channel $\mathbf{H}_{p=0}$, e.g., a line-of-sight (LoS) path that can be used for synchronization and equalization, and a channel \mathbf{H}_{tar} comprising weaker target paths indexed $p \in \mathcal{P}$ representing reflections due to objects in the surroundings. Thus, the CFR writes as

$$\begin{aligned} \mathbf{H} &= \mathbf{H}_0 + \mathbf{H}_{\text{tar}} \\ &= \alpha_0 \cdot (r_0) \mathbf{b}(f_{D,0})^T + \sum_{p \in \mathcal{P}} \alpha_p \cdot \mathbf{a}(r_p) \mathbf{b}(f_{D,p})^T + \mathbf{Z}, \end{aligned} \quad (2)$$

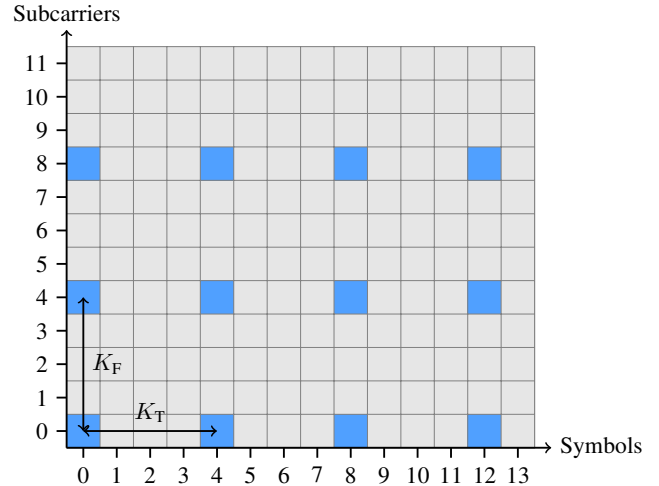


Fig. 2: Example of a hybrid resource allocation scheme, illustrated using one PRB spanning $N = 12$ subcarriers and $M = 14$ symbols. A lower MO is used on every $K_F = K_T = 4$ th Resource Element (RE) (blue squares). The remaining grey REs use a higher MO.

where the channel contributions of a path with bistatic range r_p and bistatic Doppler shift $f_{D,p}$ are described by the vectors

$$\mathbf{a}(r_p) = [1, e^{-j2\pi\Delta f \cdot r_p/c}, \dots, e^{-j2\pi(N-1)\Delta f \cdot r_p/c}]^T \quad (3)$$

$$\mathbf{b}(f_{D,p}) = [1, e^{j2\pi T_0 \cdot f_{D,p}}, \dots, e^{j2\pi(M-1)T_0 \cdot f_{D,p}}]^T, \quad (4)$$

where T_0 is the duration of an OFDM symbol and c denotes the speed of light. Note that in this work we assume perfect synchronization between TX and RX and negligible inter-carrier interference (ICI) due to Doppler shifts. In practice, sufficiently accurate synchronization could be achieved, e.g., by using a reference path as described in [5]. Moreover, while we do not make assumptions about the angular domain in this work, angular processing (e.g., beamforming) could be considered as described in [11].

III. HYBRID RESOURCE ALLOCATION SCHEME

In the following, we detail our proposed hybrid resource allocation scheme, which aims to balance the trade-off between pilots and information symbols in an ISAC context. The core idea is to not use a single, typically higher, MO Q_r for the whole data channel, but to allocate symbols with a lower MO Q_s (e.g., $Q_s = 2$ with quadrature phase-shift keying (QPSK)) as pseudo-pilots on a suitable grid for sensing. This enhances the sensing capability compared to using Q_r for the entire frame, since lower MO symbols become decodable “earlier”, i.e., at lower SNR. At the same time, the spectral efficiency reduction for the communication link is lower in comparison to using true dedicated pilots (e.g., Positioning Reference Signal (PRS) symbols) that do not convey any information. An example of one Physical Resource Block (PRB) using the proposed scheme is shown in Fig. 2, where the spacing between lower MO symbols in frequency and time, respectively denoted by K_F and K_T , is 4.

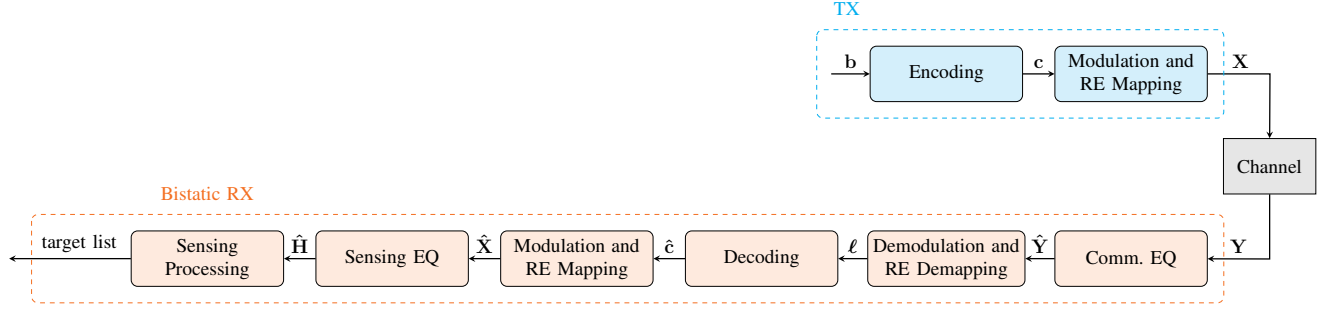


Fig. 3: Processing pipeline for bistatic sensing.

The parameters of the hybrid allocation scheme can be determined based on both communication and sensing requirements. The former must be considered as in legacy resource allocation schemes to optimize communication performance by considering KPIs like Channel Quality Indicator (CQI) or rank indicator to choose the MO Q_r for the regular data symbols (grey REs in Fig. 2). The sensing requirements include a necessary sensing link budget and sensing KPIs, e.g., unambiguous range/Doppler shift or range/Doppler shift accuracy, and depend on the use case to be supported. In a 3rd Generation Partnership Project (3GPP)-compliant system, they will likely be communicated to the sensing system by the Sensing Management Function (SeMF) in the Core Network (CN), which is foreseen to orchestrate the sensing operations.

A comprehensive analysis of how precisely the hybrid resource allocation scheme can be determined based on all the available inputs goes beyond the scope of this paper. Nonetheless, focusing only on the sensing requirements, we can formalize the following guidelines:

- 1) The required spacings K_F and K_T in frequency and time to support an unambiguous range r'_{\max} and Doppler shift $f'_{D,\max}$ can be obtained based on the well-known formulae for the maximum achievable unambiguous range r_{\max} and Doppler shift $f_{D,\max}$ [5] as follows

$$K_F = \lceil \frac{r_{\max}}{r'_{\max}} \rceil = \lceil \frac{c_0}{2\Delta f r'_{\max}} \rceil \quad (5)$$

$$K_T = \lceil \frac{f_{D,\max}}{f'_{D,\max}} \rceil = \lceil \frac{1}{2T_0 f'_{D,\max}} \rceil, \quad (6)$$

where $\lceil x \rceil$ denotes the ceil operator rounding up to smallest integer greater than or equal to x .

- 2) Similarly, the required bandwidth B and duration T_B of the sensing burst to enable a range resolution $\Delta r'$ and Doppler shift resolution $\Delta f'_D$ can be computed based on the formulae for the range resolution Δr and Doppler shift resolution Δf_D of the system [5]

$$B = \frac{c_0}{2\Delta r'} \quad (7)$$

$$T_B = \frac{1}{\Delta f'_D}. \quad (8)$$

- 3) Finally, link budget requirements should be taken into account. If the sensing burst allocation determined based

on 1) and 2) is not sufficient to support the maximum sensing range required by the use case, lower MO symbols should be allocated to additional resources to increase the processing gain.

Remark 1. *The previous guidelines are formulated based on the simplifying assumption that all lower MO pseudo-pilots will be correctly decoded at the bistatic RX, while the regular data symbols are not correctly decoded. Even though this does clearly not hold in practice, it can serve as an initial assumption that can later be refined, e.g., by observing the resulting sensing KPIs based on the used sensing burst allocation.*

The resulting spectral efficiency per symbol with our hybrid resource allocation scheme as defined in [12] is given as

$$\eta = \frac{R (N_s^{\text{RE}} Q_s + (NM - N_s^{\text{RE}}) Q_r)}{NM}, \quad (9)$$

where $N_s^{\text{RE}} = \lceil N/K_F \rceil \cdot \lceil M/K_T \rceil$ is the number of resource elements on the sensing grid. Moreover, R is the code rate, which for simplicity is assumed to be the same for the sensing grid and regular communication symbols.

IV. BISTATIC SENSING PROCESSING

Next, we describe the full processing pipeline shown in Fig. 3. Performing these operations allows us to extract sensing information at the bistatic sensing RX using our proposed hybrid resource allocation scheme. The pipeline comprises the following steps:

- **Encoding.** The information bitstream vector b to be transmitted is encoded into the codeword vector c .
- **Modulation and RE Mapping.** The codeword vector is modulated to constellation symbols using the modulation alphabets according to Q_r and Q_s . The resulting symbols are then mapped to the REs on the grid to obtain the TX frame X .
- **Channel.** The TX frame X is transmitted over the channel, which we model as described in Sec. II.
- **Comm. EQ.** Before decoding the communication signals, the RX frame Y must be equalized. As equalization (EQ) is not the focus of this work, we did not implement any channel estimation techniques based on dedicated pilot transmissions. Instead, we assume perfect knowledge of the channel of the dominant path H_0 at the RX, which can, e.g., be a LoS

path between TX and bistatic RX used for synchronization as described in [5]. Moreover, $\mathbf{H}_0 \approx \mathbf{H}$ is a fair approximation for communication. The RX frame after EQ with matrix \mathbf{G} then writes as

$$\hat{\mathbf{Y}} = \mathbf{Y}\mathbf{G}, \quad (10)$$

where ZF with the dominant path is applied. Thus,

$$[\mathbf{G}]_{n,m} = \frac{1}{[\mathbf{H}_0]_{n,m}}, \quad (11)$$

with n and m denoting subcarrier and OFDM symbol index, respectively.

• **Demodulation and RE Demapping.** The RX frame after EQ is first serialized by demapping it from the RE grid. After that, the resulting symbols are demodulated by computing the log-likelihood ratio (LLR) values ℓ .

• **Decoding.** Hard estimates of the codeword bits $\hat{\mathbf{c}}$ are obtained by decoding the LLR values ℓ .

• **Modulation and RE Mapping.** Before performing further sensing processing, the estimated codeword vector $\hat{\mathbf{c}}$ is modulated to constellation symbols and then again mapped to the RE grid to obtain the matrix containing the estimated symbols $\hat{\mathbf{X}}$. Note that this step corresponds to the step “Modulation and RE Mapping” performed at the TX.

• **Sensing EQ.** To obtain an estimate of the full channel for sensing, the transmitted symbols are equalized via ZF using the estimated symbols as

$$[\hat{\mathbf{H}}]_{n,m} = \frac{[\hat{\mathbf{Y}}]_{n,m}}{[\hat{\mathbf{X}}]_{n,m}}. \quad (12)$$

• **Sensing Processing.** Finally, the CSI matrix $\hat{\mathbf{H}}$ is processed to extract sensing information. We employ conventional 2D discrete Fourier transforms (DFTs) processing to obtain the periodogram (range-Doppler radar image) \mathbf{P} as [13]

$$[\mathbf{P}]_{n,m} = \frac{1}{N'M'} \left| \sum_{k=0}^{N'} \left(\sum_{l=0}^{M'} \hat{\mathbf{H}}(k, l) e^{-j2\pi \frac{lm}{M'}} \right) e^{j2\pi \frac{kn}{N'}} \right|^2, \quad (13)$$

where N' and M' denote the number of rows and columns of $\hat{\mathbf{H}}$ after zero padding. Note that despite the approximation $\mathbf{H}_0 \approx \mathbf{H}$, the processing gain enhances the SNR of the paths due to the focusing of the DFT operations in (13), thus also facilitating the detection of weaker target contributions in \mathbf{H}_{tar} in the periodogram. Subsequently, a cell-averaging constant false alarm rate (CA-CFAR) detector [14] is applied to obtain a list of target peaks, each characterized by a range and Doppler shift estimate.

V. RESULTS AND DISCUSSION

A. Bistatic Sensing Scenario

To assess the capability of our proposed hybrid resource allocation scheme in conjunction with the previously described

TABLE I. SIMULATION PARAMETERS.

Parameter	Value
Carrier frequency f_c	27.4 GHz
Number of subcarriers N	792
Subcarrier spacing Δf	120 kHz
Total bandwidth B	95 MHz
Number of symbols M per frame	560
Spacing in frequency K_F	4
Spacing in time K_T	4
MO for sensing grid symbols Q_s	2 (QPSK)
MO for regular data symbols Q_r	4 (16-QAM)
Code rate R	0.5
Max. iterations for BP decoding	20

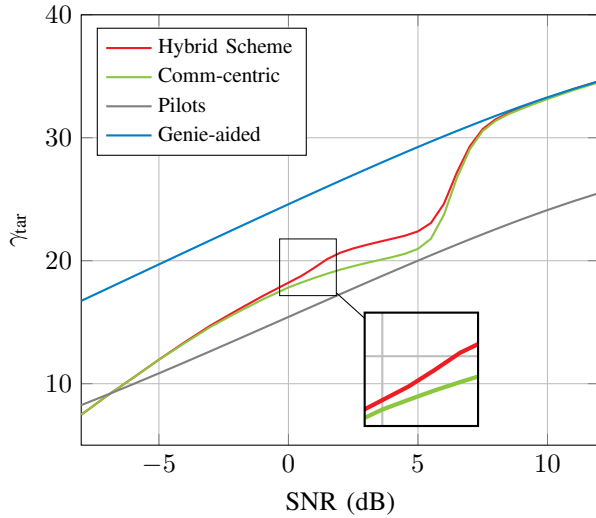
bistatic sensing processing steps, we run Monte Carlo simulations based on the system model defined in Sec. II. The simulation parameters are summarized in Table I.

In each realization, we place the dominant path at a random bistatic range r_0 between 200 and 300 m, which are typical distances in practical deployments [4]. For the $|\mathcal{P}| = 5$ point targets to be detected at the bistatic RX, excess ranges between 30 and 90 m w.r.t. the reference path are considered. This results in ranges r_p between 230 and 390 m and, disregarding radar cross-section (RCS), path losses associated with radar targets between approximately 47 to 53 dB higher than the one for the reference path. All paths are associated with a random Doppler shift f_D , with the maximum possible Doppler shift being 1.8 kHz. For comparison, this is the Doppler shift that would result from a radial velocity of 10 m/s if monostatic sensing were performed. Note that the dominant reference path is excluded from the evaluation of the sensing performance, as we assume it to be perfectly known for EQ purposes. Moreover, all random complex coefficients α include attenuation due to free space path loss.

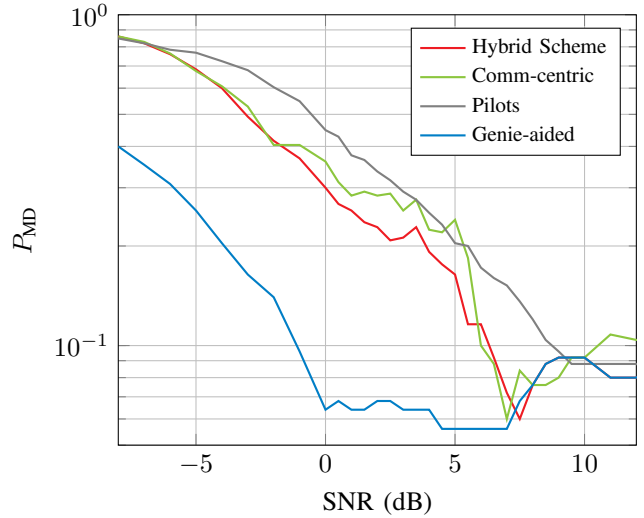
Assuming a Frequency Range 2 (FR2) setup with carrier frequency f_c and subcarrier spacing $\Delta f = 120$ kHz, each radio frame for sensing comprises $N = 792$ subcarriers and $M = 560$ symbols. For our proposed hybrid resource allocation scheme, we use the configuration depicted in Fig. 2, i.e., with spacings $K_F = K_T = 4$ and QPSK modulation ($Q_s = 2$) on the sensing grid. The remaining symbols employ 16-quadrature amplitude modulation (QAM) modulation ($Q_r = 4$). Furthermore, we use the Sionna framework [15] for channel coding. The fifth generation (5G)-compliant low-density parity-check (LDPC) channel has a code rate $R = 0.5$ and is decoded with a maximum of 20 belief propagation (BP) iterations with an early stopping criterion at the receiver. According to (9), the hybrid allocation scheme parametrized in this way achieves a spectral efficiency of $\eta_{\text{hybrid}} = 1.9375$ bits per symbol.

We evaluate the sensing performance by sweeping the SNR at the bistatic RX and examining the probability of missed detection P_{MD} and target SNR γ_{tar} . The former is the percentage of undetected targets, while we define the latter as

$$\gamma_{\text{tar}} = \frac{\sum_{p \in \mathcal{P}} [\mathbf{P}]_{k_p, l_p}}{P_{\text{res}}}, \quad (14)$$



(a) Target SNR



(b) Probability of missed detection

Fig. 4: Target SNR in the periodogram and probability of detection for our proposal “Hybrid Scheme” (red), “Comm-centric” (green), “Pilots” (grey), and “Genie-aided” (blue), both as functions of the receive SNR before radar processing.

i.e., as the ratio between the mean power of the bins with the maximum target peak contribution (i.e., one bin for each target peak) and the residual noise power P_{res} . In (14), k_p and l_p are the range and Doppler indices of the p -th target peak in the periodogram, obtained using ground truth information. Moreover, P_{res} is computed by averaging the periodogram bins that lie outside the main lobes associated with the paths. Overall, we simulate 50 realizations per SNR point. While this may seem like a relatively low number, it implies decoding ca. 85000 codewords of length 1024, which is a large enough number to gain meaningful insights into the influence of decoding errors on the sensing performance (down to a communication BLER of 10^{-3}).

We compare our proposal to the following baselines:

- **Comm-centric.** The communication-centric baseline uses 16-QAM symbols with MO $Q_r = 4$ for the whole data channel, i.e., without interleaving lower MO symbols on the sensing grid. Thus, it only aims at achieving a high spectral efficiency for the communication link without considering sensing requirements.
- **Pilots.** Sensing is performed only based on true (i.e., known) QPSK pilots that are allocated on the grid, i.e., with the same spacing $K_F = K_T = 4$.
- **Genie-aided.** The third baseline uses the same hybrid allocation scheme as our proposal, but assumes perfect knowledge of the TX data at the bistatic RX, i.e., no decoding is necessary.

B. Bistatic Sensing Performance

In the following, we restrict our evaluation to the sensing performance at the bistatic RX, i.e., we do not model and evaluate the throughput of the communication link.

Fig. 4a displays the target SNR in the periodogram γ_{tar} for our proposed hybrid scheme and the three baselines. First, one can see that “Pilots” exhibits the worst performance over

almost the whole SNR range before radar processing, which further underscores the need for sensing with the data channel to enhance the processing gain. The baseline “Genie-aided” with knowledge of the TX symbols for sensing EQ expectedly achieves the best performance. A close comparison of “Hybrid Scheme” and “Comm-centric” reveals the advantages of our proposal: around an SNR of 0 dB, a target SNR gap of up to 1.5 dB emerges between “Hybrid Scheme” and “Comm-centric”. This behavior can be attributed to the QPSK symbols we allocate on the sensing grid, which become decodable at a lower SNR compared to the 16-QAM symbols that “Comm-centric” is using for the entire data channel. The pronounced gap extends over an SNR range of ca. 6 dB, which corresponds to the expected gap between the waterfall regions for decoding QPSK and 16-QAM. For higher SNR, both “Hybrid Scheme” and “Comm-centric” converge to “Genie-aided”, as all symbols can be decoded virtually without errors.

While the probability of missed detection curves in Fig. 4b are less smooth compared to Fig. 4a due to the limited number of detections per SNR point, they show that the improved γ_{tar} translates to an enhanced target detection capability and overall confirm the previously observed trends. An improved target detection capability of “Hybrid Scheme” compared to “Comm-centric” is observed in particular in the higher SNR region.

It should be noted that the improvements come at the cost of a spectral efficiency reduction of ca. 3% (with $\eta_{\text{hybrid}} = 1.9375$ and $\eta_{\text{comm}} = 2$ bits per symbol) for the communication link. Higher gains could be achieved by using $Q_r > 4$ or if the lower MO symbols would be allocated more densely on the sensing grid by reducing K_F and K_T . Also reducing the code rate for the lower MO symbols would protect them more strongly and thus benefit sensing. However, exploring these degrees of freedom to aid symbol detection at the bistatic RX would result in a further spectral efficiency reduction for the communication

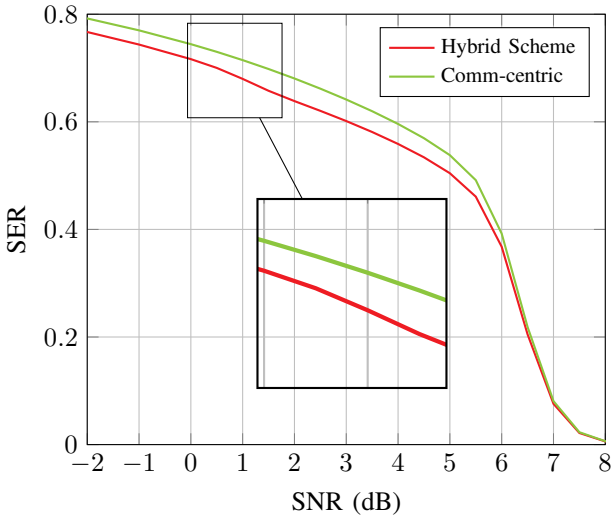


Fig. 5: Symbol error ratio (SER) at the bistatic RX for our proposal “Hybrid Scheme” (red) and “Comm-centric” (green) as function of the receive SNR before radar processing.

link. The parameter choice in practice thus requires careful consideration of the aspects described in Sec. III to trade off communication performance vs. sensing performance.

C. Impact of decoding errors on sensing performance

To get further insights into the impact of data decodability for sensing, we plot the symbol error ratio (SER) for the approaches that require decoding at the bistatic RX, i.e., our proposed hybrid scheme and the communication-centric baseline, in Fig. 5. We choose the SER as a metric over the bit error ratio (BER)/BLER metrics typically used in communications, as the SER at the bistatic RX is directly coupled to the quality of the sensing EQ and thus the quality of the CSI estimation for sensing.

One can observe that “Hybrid Scheme” achieves a lower SER than “Comm-centric” due to the QPSK symbols on the sensing grid. In line with Fig. 4, the gap widens between ca. 0 and 1.5 dB SNR, which corresponds to the waterfall region where the QPSK symbols become decodable. The seemingly minor impact on the SER curves in Fig. 5 is explained by the relatively low share of QPSK symbols, amounting to only 6.25% of all symbols. The gap closes at around 6 dB when also the 16-QAM symbols become decodable.

Together with the results from Fig. 4, the SER curves allow us to draw the following conclusions on the impact of decoding errors on the sensing performance: sensing using the data channel does not necessarily require correct decoding of the entire frame. Rather, each correctly decoded symbol benefits the CSI estimation, comparable to a processing gain due to more available REs. Decoding errors therefore appear to have no direct detrimental effect on sensing apart from a reduced processing gain, as long as they are random and do not exhibit specific patterns as discussed in [5].

VI. CONCLUSION

In this paper, we proposed a hybrid resource allocation scheme to facilitate bistatic sensing operations using data channels. By allocating lower MO symbols as “pseudo-pilots” on a suitable grid for sensing, we facilitate the correct decoding of the data channel symbols at the bistatic RX. Our simulation results show that using the resulting improved CSI matrix estimation for sensing leads to a higher target SNR in the radar image accompanied by an improved detection performance compared to the communication-centric baseline. Moreover, we drew conclusions about the impact of the decoding errors on the sensing performance. Future work should include a more extensive exploration of the various degrees of freedom for the hybrid resource allocation scheme, as well as a holistic investigation that also considers the performance of the communication link.

ACKNOWLEDGMENTS

The authors acknowledge the financial support by the Federal Ministry of Research, Technology and Space of Germany in the project “SENSATION” under grant number 16KIS2523K.

REFERENCES

- [1] N. González-Prelcic *et al.*, “The Integrated Sensing and Communication Revolution for 6G: Vision, Techniques, and Applications,” *Proc. IEEE*, vol. 112, no. 7, pp. 676–723, Jul. 2024.
- [2] A. Ghosh *et al.*, “A Unified Future: Integrated Sensing and Communication (ISAC) in 6G,” *IEEE J. Sel. Topics Electromagn. Antennas Propag.*, Aug. 2025.
- [3] S. Mandelli, M. Henninger, M. Bauhofer, and T. Wild, “Survey on Integrated Sensing and Communication Performance Modeling and Use Cases Feasibility,” in *2nd Int. Conf. 6G Netw.*, Oct. 2023, pp. 1–8.
- [4] L. Giroto *et al.*, “Bistatic ISAC: Practical Challenges and Solutions,” *arXiv preprint*, Jan. 2026.
- [5] D. Brunner *et al.*, “Bistatic OFDM-Based ISAC With Over-the-Air Synchronization: System Concept and Performance Analysis,” *IEEE Trans. Microw. Theory Techn.*, vol. 73, pp. 3016–3029, May 2025.
- [6] K. M. Braun, “OFDM Radar Algorithms in Mobile Communication Networks,” Ph.D. dissertation, Karlsruher Institut für Technologie, 2014.
- [7] K. Han, K. Meng, A. Chatzicharistou, and C. Masouros, “Constellation Design in OFDM-ISAC over Data Payloads: From MSE Analysis to Experimentation,” *arXiv preprint arXiv:2510.13101*, Oct. 2025.
- [8] A. Gupta, P. Ganji, S. Srivastava, and A. K. Jagannatham, “Data-Aided Bistatic Sensing and Communication for mmWave MIMO-OFDM ISAC Systems,” *IEEE Trans. Commun.*, vol. 73, pp. 9720–9734, Oct. 2025.
- [9] M. F. Keskin, S. Mura, M. Mitzmizi, D. Tagliaferri, and H. Wymeersch, “Bridging the Gap via Data-Aided Sensing: Can Bistatic ISAC Converge to Genie Performance?” in *IEEE Radar Conf.*, Oct. 2025, pp. 514–519.
- [10] D. Bao, G. Qin, and Y.-Y. Dong, “A Superimposed Pilot-Based Integrated Radar and Communication System,” *IEEE Access*, vol. 8, pp. 11 520–11 533, Jan. 2020.
- [11] A. Felix, S. Mandelli, M. Henninger, and S. ten Brink, “Optimal Azimuth Sampling and Interpolation for Bistatic ISAC Setups,” in *28th Int. Workshop Smart Antennas (WSA)*, Sep. 2025.
- [12] 3GPP, “NR; Physical layer procedures for data,” Technical Specification (TS) 38.214, 2025, version 19.1.0.
- [13] M. Braun, C. Sturm, and F. K. Jondral, “Maximum Likelihood Speed and Distance Estimation for OFDM Radar,” in *IEEE Radar Conf.*, May 2010, pp. 256–261.
- [14] M. A. Richards, J. A. Scheer, and W. A. Holm, *Principles of Modern Radar: Basic Principles*. Raleigh, NC, USA: SciTech Pub., 2010.
- [15] J. Hoydis *et al.*, “Sionna: An open-source library for next-generation physical layer research,” *arXiv:2203.11854*, 2022.